High quality factor photonic resonators for nitride quantum dots

T. Guillet[*,1], **M. Mexis**[1,2], **S. Sergent**[3,4], **D. Néel**[5], **S. Rennesson**[1,2], **C. Brimont**[1,2], **T. Bretagnon**[1,2], **B. Gil**[1,2], **D. Sam-Giao**[6], **B. Gayral**[6], **F. Semond**[3], **M. Leroux**[3], **S. David**[5], **X. Checoury**[5], and **P. Boucaud**[5]

[1] Université Montpellier 2, Laboratoire Charles Coulomb UMR 5221, 34095 Montpellier, France
[2] CNRS, Laboratoire Charles Coulomb UMR 5221, 34095 Montpellier, France
[3] CRHEA-CNRS, Valbonne 06560, France
[4] Université de Nice Sophia Antipolis, Parc Valrose, Nice 06102 Cedex 2, France
[5] Institut d'Electronique Fondamentale, CNRS – Université Paris Sud 11, 91405 Orsay, France
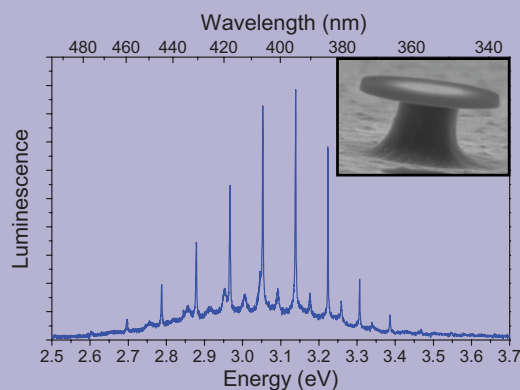[6] CEA-INAC, 17 rue des Martyrs, 38054 Grenoble, France

* Corresponding author: e-mail thierry.guillet@univ-montp2.fr, Phone: +00 33 4 67 14 37 89, Fax: +00 33 4 67 14 37 60

We report the realization and the optical study of nitride photonic resonators dedicated to the blue and UV spectral range. Microdisks and photonic crystal (PC) cavities are investigated containing GaN/AlN quantum dots (QDs) embedded in an AlN waveguide. The PC cavities are fabricated through the conformal growth of nitrides on a patterned Si substrate, and present delocalized and confined cavity modes in their microphotoluminescence spectra, that are compared to simulations. A large quality factor of 1800 is reached for a modified L3 cavity. In the case of microdisks, which are fabricated through a classical top-down approach, the series of whispering gallery modes (WGMs) with large quality factors (up to 7300) are observed and analysed.

Scanning electron micrograph and microphotoluminescence spectrum of a 2 μm AlN microdisk embedding GaN QDs; the WGMs appear as sharp peaks, with quality factors up to 5000.

1 Introduction III-N materials have become the dominant materials for UV to blue–green semiconductor light sources. Besides these conventional light emitters, group III-nitride (III-N) materials are also attracting candidates for less conventional emitters and for new applications (integration with electronics, lab-on-chip, array of microsources...) [1–3]. In order to better control the light emission in the UV spectral range, various optical resonators are presently investigated, based on GaN or ZnO nanostructures: Fabry–Perot modes in planar microcavities and in nanowires [4–10], whispering gallery modes (WGMs) in microwires [11] and microdisks [12–15], cavities in photonic crystal (PC) membranes [16–19], as well as random lasing in powders [20] and waveguides [21]. Realizing photonic nanostructures with large quality factors in the UV range is challenging due to the larger scattering losses compared to similar structures in the visible and IR spectral ranges. This is especially important in the case of PC cavities, where the period of the PC is reduced to the order of 150 nm. Up to now, the light emitters have been chosen according to their large density of states for excitons (bulk GaN and ZnO for near UV operation) or to the tunability of their

wavelength (InGaN/GaN quantum wells for blue operation). For room temperature operation, nitride quantum dots (QDs) are promising candidates due to their large radiative efficiency, as shown recently for GaN/(Al,Ga)N QDs grown on Si substrates [22–24]. The single dot emission of similar QDs has been studied in samples with a more dilute QD concentration, and spectral diffusion effects as well as a strong polarization of the luminescence of each QD have been evidenced [25, 26].

In this work, we study the optical properties of (Al,Ga)N photonic resonators – PC membrane cavities as well as microdisks – embedding GaN QDs. The QD concentration is large, so that each photonic mode is coupled to an ensemble of resonant QDs. In photonic cavities, we have identified the delocalized slow modes of the PC as well as the confined modes of the cavities. Their quality factors reach 1800. In the case of microdisks, we have observed and modelled the optical modes, with promising quality factors ranging from 1000 to 7300.

2 Photonic crystal nanocavities The realization of AlN PC membranes is challenging due to the chemical inertness of AlN. In order to circumvent the problem of AlN etching, an original approach is proposed, that is based on the conformal growth of AlN on a patterned Si substrate [27]. The photonic pattern is first defined by electron-beam lithography and shallow etching on the Si (111) substrate. The two dimensional conformal epitaxy of AlN on Si has then been optimized [23, 24, 28] in order to reliably reproduce the photonic pattern. The thickness of the AlN layer (70 nm) is chosen to allow monomode guiding of the light in the membrane. A freestanding membrane is finally obtained by selective etching of the Si substrate. Figure 1 presents the sample structure and the top SEM images of H1 and modified H2 cavities. The period of the crystal is $a = 170$ nm and the radius of the holes is $r = 50$ nm, in order to obtain a photonic band gap around $\lambda = 400$ nm. The H1 cavity consists of a single missing hole in the PC pattern. In the modified H2 cavity, this missing hole is surrounded by six smaller holes (radius $r \approx 15$ nm), such that the confined mode has a larger nominal quality factor.

A single plane of GaN/AlN QDs is embedded in the middle of the AlN layer. They present an emission spectrum centred at 3.2 eV, having a large linewidth due to the height distribution of the QDs. Indeed the built-in electric fields in such polar QDs imply a strong variation of the transition energy when the height of the dots is varied [29].

The spectroscopy of the PC nanocavities is probed by micro-photoluminescence (μPL) experiments. The sample is excited at room temperature with a 266 nm CW laser (Crylas/FQCW 266-50). The excitation power density is about 100 W cm^{-2}. The emission is analysed by a 55 cm spectrometer with a liquid nitrogen-cooled CCD. Figure 2 presents the μPL spectra recorded for the H1 and modified H2 cavities shown in the Fig. 1. The spectra consist of a 1 eV broad peak, and few sharp peaks. The broad peak is similar to the one measured on unprocessed parts of the sample, and
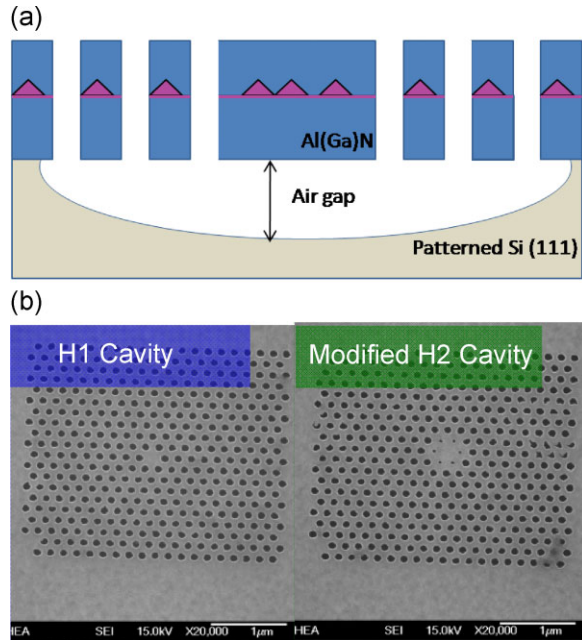

Figure 1 (online colour at: www.pss-b.com) (a) Schematic cross-section of the freestanding PC membrane; (b) SEM images of two cavities H1 (1 missing hole) and H2 modified (one missing hole surrounded by six small holes).
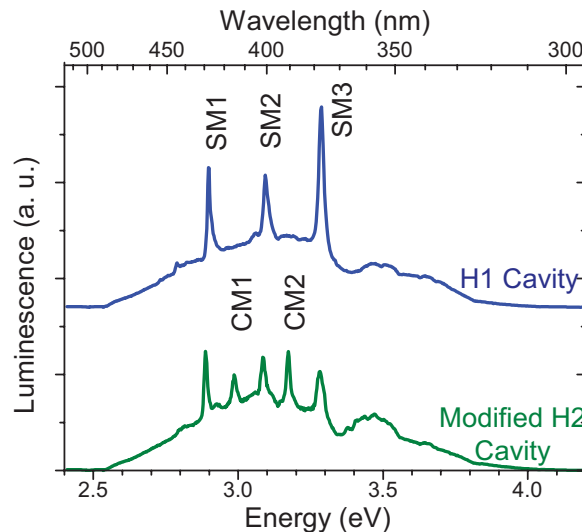

Figure 2 (online colour at: www.pss-b.com) μPL spectra of the H1 and modified H2 cavities ($T = 300$ K).

therefore reflects the photoluminescence of the embedded QDs. Three of the sharp peaks (named SM1-3) are observed for all PC cavities, whatever the shape of the cavity defect. The spectrum of the modified H2 cavity presents two additional peaks (named CM1 and CM2), that are specific to each pattern and are a signature of perfectly realized cavities.
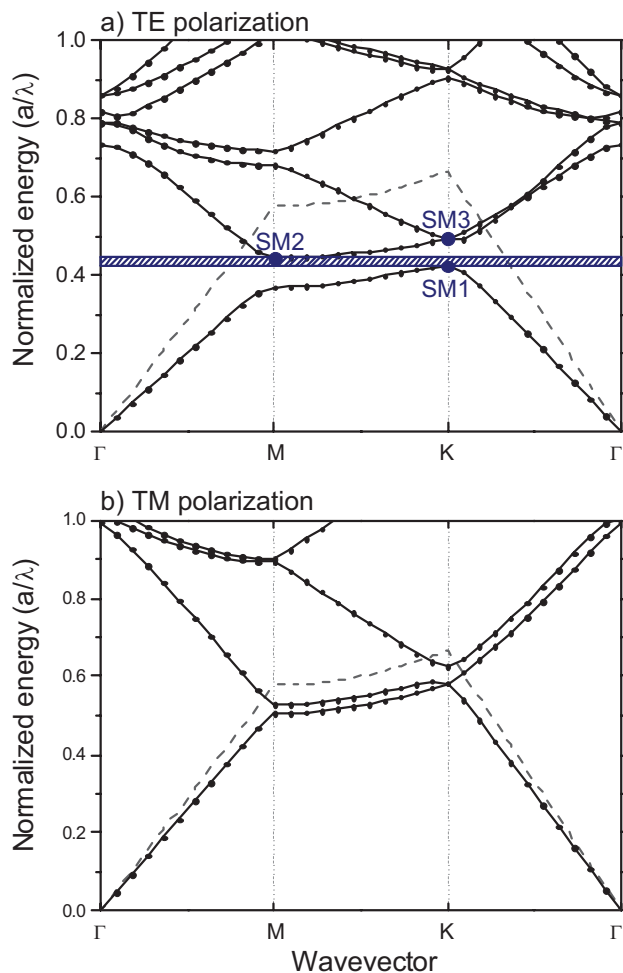
Phys. Status Solidi B **249**, No. 3 (2012)

451

Original

Paper

Figure 3 Simulated band structure calculated by the plane wave expansion method in (a) TE and (b) TM polarizations. A photonic band gap is obtained in TE polarization, shown as a dashed area. The slow modes at band extrema are also indicated, as well as the light cone (dashed line).

Figure 4 (online colour at: www.pss-b.com) (a) Scanning electron micrograph of an L3 cavity with 20% displaced edge holes; (b) μPL high-resolution spectrum of this cavity at room temperature; the inset presents the enlarge spectrum of the fundamental mode CM1 with a Lorentzian fit.

The experimental results are compared to the band dispersions calculated for a 2D PC without a cavity, as shown in Fig. 3. The design of the crystal (i.e. the period a and the ratio r/a) has been optimized to obtain the largest photonic band gap (about 190 meV) centered around $\lambda = 400$ nm in TE polarization. Three band extrema are identified in Fig. 3(a), whose energies are equal to 2.90, 3.09 and 3.28 eV. They correspond to the energies of the three peaks observed for all investigated cavities; those are therefore attributed to the slow modes of the 2D PC (SM1-3), that are delocalized in the whole PC area. The additional peaks CM1 and CM2 observed on the modified H2 cavity are between the energies of the slow modes and are specific to each cavity. They are attributed to cavity modes that are confined around the PC defect. Their measured quality factors are equal to 350, and are probably limited by the small size of the PC surrounding the cavity and to their roughness.

In order to enhance the quality factor of the PC cavities, the design of L3 cavities (3 in-line missing holes) has then
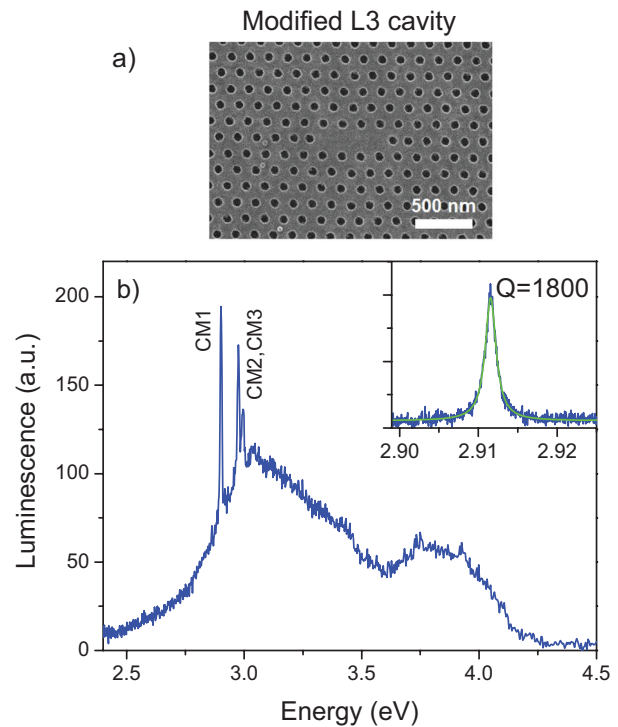
been optimized by shifting the edge air holes with respect to the initial lattice (Fig. 4(a)). This hole displacement improves the confinement of the cavity mode inside the dielectric material, as previously shown for silicon-based PCs [30]. The AlN waveguide is here 100 nm thick and embeds two planes of GaN QDs. As opposed to the previous example, the conformal growth was performed in two steps: a 15 nm thick AlN membrane was first deposited [27]. Underetching of silicon was then performed using a HF/nitric acid/acetic acid solution. Following this underetch step, a 85 nm thick AlN layer containing the QD planes was then grown. This procedure allows to minimize the occurence of vertical sidewalls under the membrane, that might be present when growing a thick AlN membrane.

The μPL spectrum of a modified L3 cavity obtained by this method is presented in the Fig. 4(b). Three modes are observed between 2.91 and 3 eV. Their energies and amplitudes depend on the value of the hole displacement, for various cavities realized on the same sample, showing that the modes are related to the cavity and not to slow modes of the surrounding PC. The fundamental mode of the cavity, at low energy, has an optimal contrast for a hole displacement of 20%, and its quality factor reaches 1800. This value is comparable to the state of the art for nitride PC cavities [17]. The comparison between experimental spectra and simulations by three-dimensional finite-difference in

time domain calculations (3D-FDTD) is presented in Ref. [27]. The simulated quality factor for this cavity is equal to 4800. The difference with the experimental value is attributed to the roughness and imperfections of the AlN PC membrane.

3 Microdisks As in the case of PC cavities, the samples consist in a patterned AlN waveguide embedding GaN/AlN QDs. The whole nitride structure is first grown on the Si substrate. 4 QD planes are grown on a 35-nm-thick AlN buffer layer, separated by 10-nm-thick AlN spacers. They are then capped by a 35-nm-thick AlN layer, so that the overall nitride waveguide is 110 nm thick. The microdisks are then defined by electron-beam lithography, and etched down to the Si substrate by reactive ion etching (Fig. 5(a)) [31]. The etching of the nitride layer is here more appropriate than in the case of PC membranes since it is applied to large areas. The post is finally realized by selective wet chemical etching of the Si substrate. A scanning electron micrograph of a 2 μm microdisk is shown in the Fig. 5(b). Details on the fabrication process are reported in [31].

The μPL spectra of two microdisks with different diameters are presented in the Fig. 6. The WGMs emission can be collected from the top if the light is scattered by defects on the microdisk, or from the edge if the light tunnels out of the microdisk. In our case, the μPL set-up is used for excitation of a single microdisk, and the collection is performed from the edge with a lens and a multi-mode optical fibre, leading to a better contrast of the peaks corresponding to the WGMs. As in the case of PC cavities, the spectra are composed of a spectrally broad emission corresponding to the embedded QDs, and a series of peaks corresponding to WGMs. The high quality of the microdisks and the low absorption of the QDs allow to observe periodic series of sharp peaks, corresponding to WGMs with the same radial order and a different azimuthal order, in contrast with previous studies on nitride microdisks [12–15]. Figure 6(c) presents a high-resolution spectrum (grating with 3600 lines mm^{-1}, resolvance 20,000) of the 2 μm microdisk. The sharpest peaks have Q factors larger than 3000 and are attributed to first order radial modes. Their emissions are weaker than the ones of the second order radial modes, with
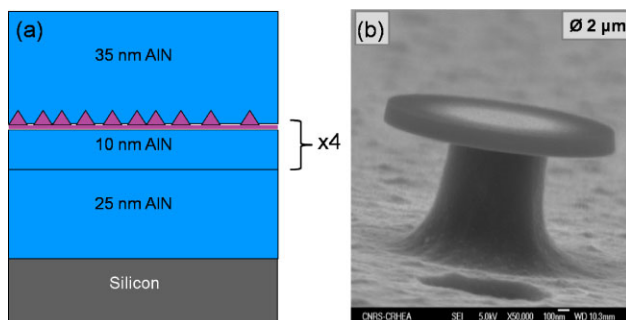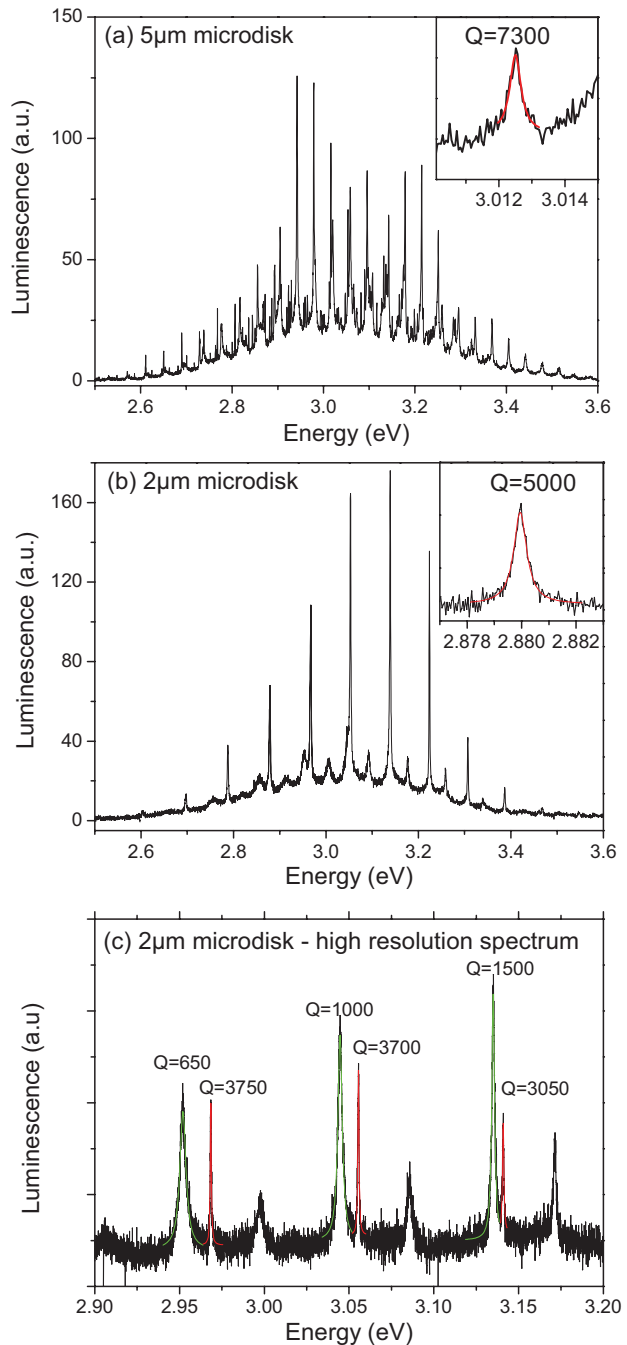

Figure 6 (online colour at: www.pss-b.com) Microphotoluminescence spectra of a 5 μm (a) and a 2 μm (b) microdisk at $T = 300$ K; the insets present the Lorentzian fit of the peak with the highest quality factor. (c) High resolution spectrum of the same 2 μm microdisk, with Lorentzian fits of first (red) and second (green) radial order modes.

Q factors of the order of 1000. This is related to the larger mode extension of the second order radial modes inside the microdisk, and therefore the larger number of resonant photoexcited QDs. The quality factors of 5 μm microdisks are larger than the ones observed for 2 μm microdisks, and
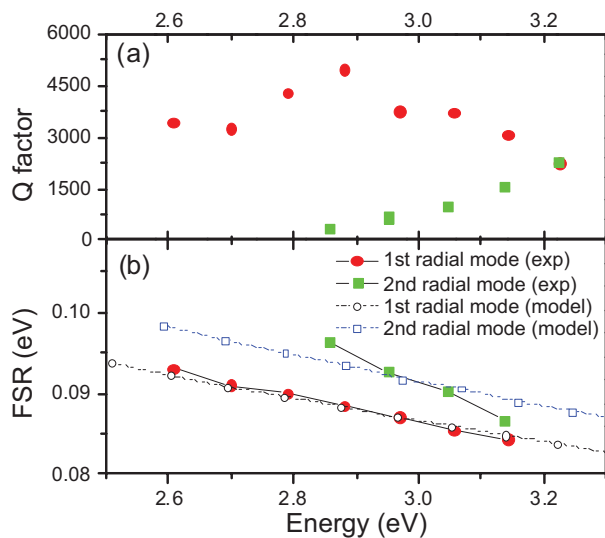

Figure 5 (online colour at: www.pss-b.com) (a) Epitaxial structure of the microdisk; (b) SEM image of a 2 μm microdisk.

Phys. Status Solidi B **249**, No. 3 (2012)

Original

Paper

453

Figure 7 (online colour at: www.pss-b.com) (a) Quality factor and (b) FSR of the first and second radial order modes, measured for the 2 μm microdisk corresponding to the Fig. 5(b). The FSRs calculated for a 2.06 μm microdisk are indicated as open circles and dashed lines.

reach 7300 for the sharpest peaks (Fig. 6(a), inset). This is presently the largest reported Q value for nitride photonic resonators.

The analysis of the periodicity and the quality factor of the modes is presented in the Fig. 7. Each peak is well fitted with a Lorentzian lineshape, allowing a precise determination of the quality factor. In order to confirm the assignment of the peaks to first and second order radial modes, the free spectral range (FSR) is compared with a numerical model based first on the calculation of the guided modes in a standard planar 1-D waveguide [32] and then on solving the Maxwell equations across a boundary of cylindrical symmetry [33]. The spectral dependence of the effective refractive index is taken into account. Only TE modes are considered, corresponding to the predominant polarization of the observed WGMs. A very good agreement is found for a microdisk diameter of 2.06 μm.

The spectral dependence of the Q factors reflects the processes limiting it. For first radial order modes, no strong dependence is found below 3.05 eV, and the Q factors are of the order of 3000 to 5000, well below the limit induced by the tunneling out of a perfect microdisk (more than 10^4 for such microdisks). It is therefore attributed to a slight contribution of scattering processes at the surface or the periphery of the microdisk, even though efforts have been done to limit their roughness [31]. On the high-energy side of the spectrum, the progressive decrease of the Q factor could reflect the onset of the QD absorption. The increase of the Q factor of second order modes is more intriguing. It has been recently shown that it is due to the larger overlap of those modes with the strongly absorbing Si post, which increases at longer wavelengths [34].

4 Conclusion We have demonstrated two approaches for the realization of photonic resonators with large quality factors in the blue and UV spectral range. They are based on GaN/AlN QDs exhibiting high photoluminescence efficiency at room temperature. PC cavities have been developed by an original process based on the conformal growth of nitrides on a patterned Si substrate. The delocalized slow modes of the PC as well as the confined modes of the cavities have been identified. For L3 cavities with displaced edge holes, we have obtained a large quality factor of 1800. The microdisks present even higher quality factors, up to 7300. Their spectra are composed of series of sharp peaks corresponding to mode families. This allows modelling and analysing their FSR and quality factor, which are related to their intrinsic properties.

References

[1] H. Jiang, S. Jin, J. Li, J. Shakya, and J. Lin, Appl. Phys. Lett. **78**, 1303 (2001).
[2] S. Krawczyk, Phys. Status Solidi C **0**, 998 (2003).
[3] H. Craighead, Nature **442**, 387 (2006).
[4] S. Kako, T. Someya, and Y. Arakawa, Appl. Phys. Lett. **80**, 722 (2002).
[5] J. C. Johnson, H.-J. Choi, K. P. Knutsen, R. D. Schaller, P. Yang, and R. J. Saykally, Nature Mater. **1**, 106 (2002).
[6] S. Gradecak, F. Qian, Y. Li, H.-G. Park, and C. M. Lieber, Appl. Phys. Lett. **87**, 173111 (2005).
[7] Y. Higuchi, K. Omae, H. Matsumura, and T. Mukai, Appl. Phys. Express **1**, 121102 (2008).
[8] G. Christmann, R. Butté, E. Feltin, J.-F. Carlin, and N. Grandjean, Appl. Phys. Lett. **93**, 051102 (2008).
[9] M. A. Zimmler, F. Capasso, S. Müller, and C. Ronning, Semicond. Sci. Technol. **25**, 024001 (2010).
[10] T. Guillet, C. Brimont, P. Valvin, B. Gil, T. Bretagnon, F. Médard, M. Mihailovic, J. Zúñiga-Pérez, M. Leroux, F. Semond, and S. Bouchoule, Appl. Phys. Lett. **98**, 211105 (2011).
[11] L. Sun, Z. Chen, Q. Ren, K. Yu, L. Bai, W. Zhou, H. Xiong, Z. Q. Zhu, and X. Shen, Phys. Rev. Lett. **100**, 156403 (2008).
[12] S. Chang, N. B. Rex, R. K. Chang, G. Chong, and L. J. Guido, Appl. Phys. Lett. **75**, 166 (1999).
[13] H. W. Choi, K. N. Hui, P. T. Lai, P. Chen, X. H. Zhang, S. Tripathy, J. H. Teng, and S. J. Chua, Appl. Phys. Lett. **89**, 211101 (2006).
[14] A. C. Tamboli, E. D. Haberer, R. Sharma, K. H. Lee, S. Nakamura, and E. L. Hu, Nature Photon **1**, 61 (2007).
[15] D. Simeonov, E. Feltin, A. Altoukhov, A. Castiglia, J.-F. Carlin, R. Butté, and N. Grandjean, Appl. Phys. Lett. **92**, 171102 (2008).
[16] Y.-S. Choi, K. Hennessy, R. Sharma, E. Haberer, Y. Gao, S. P. DenBaars, S. Nakamura, E. L. Hu, and C. Meier, Appl. Phys. Lett. **87**, 243101 (2005).
[17] M. Arita, S. Ishida, S. Kako, S. Iwamoto, and Y. Arakawa, Appl. Phys. Lett. **91**, 051106 (2007).

[18] T. N. Oder, K. H. Kim, J. Y. Lin, and H. X. Jiang, Appl. Phys. Lett. **84**, 466 (2004).

[19] S. W. Chen, T. C. Lu, Y. J. Hou, T. C. Liu, H. C. Kuo, and S. C. Wang, Appl. Phys. Lett. **96**, 071108 (2010).

[20] J. Fallert, R. J. B. Dietz, J. Sartor, D. Schner, C. Klingshirn, and H. Kalt, Nature Photon **3**, 279 (2009).

[21] P.-H. Dupont, C. Couteau, D. J. Rogers, F. H. Teherani, and G. Lerondel, Appl. Phys. Lett. **97**, 261109 (2010).

[22] J. Renard, P. K. Kandaswamy, E. Monroy, and B. Gayral, Appl. Phys. Lett. **95**, 131903 (2009).

[23] S. Sergent, B. Damilano, T. Huault, J. Brault, M. Korytov, O. Tottereau, P. Vennegues, M. Leroux, F. Semond, and J. Massies, J. Appl. Phys. **109**, 053514 (2011).

[24] S. Sergent, J.-C. Moreno, E. Frayssinet, S. Chenot, M. Leroux, and F. Semond, Appl. Phys. Express **2**, 051003 (2009).

[25] R. Bardoux, T. Guillet, P. Lefebvre, T. Taliercio, T. Bretagnon, S. Rousset, B. Gil, and F. Semond, Phys. Rev. B **74**, 195319 (2006).

[26] R. Bardoux, T. Guillet, B. Gil, P. Lefebvre, T. Bretagnon, T. Taliercio, S. Rousset, and F. Semond, Phys. Rev. B **77**, 235315 (2008).

[27] D. Néel, S. Sergent, M. Mexis, D. Sam-Giao, T. Guillet, C. Brimont, T. Bretagnon, F. Semond, B. Gayral, S. David, X. Checoury, and P. Boucaud, Appl. Phys. Lett. **98**, 261106 (2011).

[28] J. Moreno, E. Frayssinet, F. Semond, M. Placidi, and P. Godignon, Mater. Sci. Semicon. Process. **12**, 31 (2009).

[29] T. Bretagnon, P. Lefebvre, P. Valvin, R. Bardoux, T. Guillet, T. Taliercio, B. Gil, N. Grandjean, F. Semond, B. Damilano, A. Dussaigne, and J. Massies, Phys. Rev. B **73**, 113304 (2006).

[30] Y. Akahane, T. Asano, B.-S. Song, and S. Noda, Nature **425**, 944 (2003).

[31] S. Sergent, J. C. Moreno, E. Frayssinet, Y. Laaroussi, S. Chenot, J. Renard, D. Sam-Giao, B. Gayral, D. Néel, S. David, P. Boucaud, M. Leroux, and F. Semond, J. Phys. Conf. Ser. **210**, 012005 (2010).

[32] A. Yariv, Optical Electronics, 4th edn. (Saunders College Publishing, Orlando, 1995).

[33] M. Borselli, T. Johnson, and O. Painter, Opt. Express **13**, 1515 (2005).

[34] M. Mexis, S. Sergent, T. Guillet, C. Brimont, T. Bretagnon, B. Gil, F. Semond, M. Leroux, D. Néel, S. David, X. Checoury, and P. Boucaud, Opt. Lett. **36**, 2203 (2011).